Analysis Note

Directed flow v_1 of deuterons in the Xe+Cs(I) collisions at 3.8 AGeV (BM@N run8)

Irina Zhavoronkova[1], Mikhail Mamamev[2], Arkadiy Taranenko[3], Alexander Demanov, Petr Parfenov, Valery Troshin.
National Research Nuclear University MEPhI, Moscow, Russia
Joint Institute for Nuclear Research, Dubna, Russia
Institute for Nuclear Research of the Russian Academy of Sciences, Moscow, Russia

---

In this note, we present the directed flow v_1 measurements of protons from Xe+Cs(I) collisions at 3.8 AGeV (BM@N run8). We show the datasets, event and track selection cuts, centrality definition, event plane reconstruction and resolution. The v_1 results are presented as function of transverse momentum (p_T) and rapidity (y_{cm}) for 10-30% central Xe+Cs(I) collisions. The systematic uncertainty study will also be presented and discussed. The v_1 measurements are compared with results of JAM transport model calculations and published data from other experiments.

---

[1]E-mail: irina.calv.45@gmail.com
[2]E-mail: mam.mih.val@gmail.com
[3]E-mail: AVTaranenko@mephi.ru

Contents

1 Introduction

Collective motion of particles produced in heavy ion collisions is the result of the evolution of the initial spatial asymmetry of matter created in the overlap region. This evolution occurs by the means of the interaction of the constituents of the matter with each other and with cold spectator fragments. Thus the final-state momentum anisotropy reflects the underlying properties of strongly interacting matter and is sensitive to the baryon densities and temperatures achieved in the collision. This momentum anisotropy is usually quantified with the Fourier-decomposition of the azimuthal angle distribution of the produced in the collision particles with respect to the reaction plane Ψ_{RP}, spanned on the vectors of impact parameter and beam direction [1; 2]:

$$\frac{dN}{d\varphi} \propto \frac{1}{2\pi}(1 + 2\sum_{n=1}^{\infty} v_n \cos n(\varphi - \Psi_{RP})), \tag{1}$$

where φ is the particles azimuthal angle and coefficients v_n calculated as:

$$v_n = \langle \cos n(\varphi - \Psi_{RP}) \rangle, \tag{2}$$

where angle brackets denote the average over all azimuthal and reaction plane angles.

Coefficients v_n, usually referred to as anisotropic flow of n-th harmonic played an important role in discovering the properties of strongly interacting quark-gluon matter (QGM) at top RHIC and LHC energies. Using the data for the elliptic flow v_2, it was shown that QGM posses the lowest known shear viscosity η/S [3].

At lower beam energies of several GeV per nucleon the passing time of the colliding nuclei is comparable to the time of the evolution of the matter within the overlapping region. Therefore interaction of the produced in the collision matter with cold spectator matter provides the significant contribution the final values of anisotropic flow [4]. The particle emission pattern changes flow in-plane to out-of-plane when going down the collision energy [5]. Additionally, presence of the spectator matter during the evolution of the matter within the overlapping region leads to achieving higher net-baryon densities exceeding by the factor of 3-5 that of regular nuclear matter [6]. Matter under such extreme conditions may be found in

the compact stellar objects such as neutron stars [7]. Studying the anisotropic flow of the produced in the collision particles may shed light on the properties of strongly interacting matter at these conditions and help to establish the equation of state (EOS) at the region of high net-baryon densities.

The mechanisms of light nuclei production in heavy-ion collisions at the region of beam energy of several A GeV is not fully understood. However, the recent findings of the STAR collaboration tend to favor the coalescence mechanism over others [8]. In this model, the light nuclei are produced via binding of nucleons which are close in momentum space, which leads to the scaling of the directed flow:

$$v_1^p(p_T) \approx v_1^d/2(p_T/2) \approx v_1^t/3(p_T/3). \tag{3}$$

The Baryonic Matter at the Nuclotron (BM@N)[9] is a fixed target experiment at JINR (Dubna). In February 2023, the first physics run of the BMN experiment was completed with recorded Xe + Cs(I) collision events at $E_{beam} = 3A$ GeV ($\sqrt{s_{\rm NN}}$= 3.02 GeV) and 3.8A GeV ($\sqrt{s_{\rm NN}} = 3.26$ GeV). In this analysis note, we present first results on directed flow (v_1) of protons in 10-30% central Xe + Cs(I) collisions at $E_{beam} = 3.8A$ GeV. The analysis presented bellow is based on the analysis performed for the directed flow of protons. The data selection criteria and symmetry plane estimation are carried out identically to [10]. While the approach for deuteron selection and systematic error evaluation is similar to how it was done for protons, there will be a slight variations. The note is organized as follows. Section 2 is dedicated to event and track selection. Section 3 briefly describes the methods used for analysis of the directed flow of deuterons. In section 4 we present the study for the systematic uncertainty. Finally, Section 5 presents the main results on directed flow v_1 of deuterons.

2 Data, Event and Track Selection

In total approximately 500 million events of Xe+Cs(I) collisions at the beam energy of 3.8A GeV were collected by the BM@N experiment in the January of 2023. The event selection procedure is identical to how it was done for proton directed flow analysis. Bellow we briefly remind the selection criteria employed. For further details see [10].

1. We don't consider runs below RunId=6924 due to unstable operation of the GEM and FSD detectors (BM@N Electronic Logbook).

2. We removed 74 runs [18M events] based on QA study (see our previous analysis note [10])

3. We used events from Physical runs and CCT2 trigger [9].

4. At least 2 tracks in vertex reconstruction

5. The pileup events were rejected based on the $\pm 3\sigma$ cut on the correlation between the number of FSD digits and the number of charged particles in the tracking system (FSD + GEM).

Table 1: Statistics after applying the selection criteria

Cuts	no. of events	%
def.	530 M	100%
CCT2 trigger	437 M	82%
at least 2 tracks in vertex reconstruction	315 M	59%
Pileup rejection cuts	285 M	53%
QA study	267 M	50%

Selection criteria are also imposed on tracks to ensure good tracks for analysis. The selection cuts applied are as follows:

1. Tracks of charged particles were selected based on the number of stations N_{hits} in the BM@N inner tracking system used for track reconstruction. At least 6 were required to satisfy the criteria of a good track: $N_{hits} > 6$.

2. Only tracks with fit quality $\chi^2/NDF < 5$ were analyzed.

3. Distance of the closest approach (DCA) of tracks from the primary vertex in the direction perpendicular to the beam: DCA < 5 cm

Deuterons are identified using the time of flight Δt measured between T0 and the ToF detectors, the length of the trajectory ΔL and the momentum p reconstructed in the BM@N central tracker. Then the squared mass m^2 of a particle is calculated. Figure 1 shows the population of the positively charged particle in the plane spanned by their square mass m^2 and rigidity (p/q) for the TOF400 and TOF700. For each bin in momentum the position $\langle m_d^2 \rangle$ and the width $\sigma_{m_d^2}$ of the deuteron m^2 peak was extracted from the Gaussian fit. The procedure was done separately for TOF-400 and TOF-700 as they have different timing resolution. The proton peak was approximated with gaussian fit as well to calculate the possible contamination and to develop the adequate selection criteria to maximize the deuteron purity. Figure 2 shows the m^2 distribution of particles detected in the TOF700 for the particular momenta from the different momentum. Red curves are approximations of the proton and deuteron peaks, and dashed vertical lines indicate the m^2 range in which the particles are selected as deuterons.

m^2 ranges for different momentum windows used in the analysis are shown in Table 2.

p/q	$m^2 - \langle m^2 \rangle$	
	TOF400	TOF700
0–4 GeV/c	(-3σ, 3σ)	(-2σ, 3σ)
4–6 GeV/c	(-2σ, 3σ)	(-1σ, 3σ)
6–8 GeV/c	(-1σ, 3σ)	(0, 3σ)

Table 2: Deuteron selection criteria based on the square mass m^2 in different rigidity (p/q) ranges.

On Figure 4 shown are the selected deuterons in the m^2 vs. p/q plane for the TOF400 and TOF700 detectors. Figure 5 shows the m^2 distribution of all particles detected in the TOF700 and of the selected deuterons for different y and p_T bins, used in the analysis further.

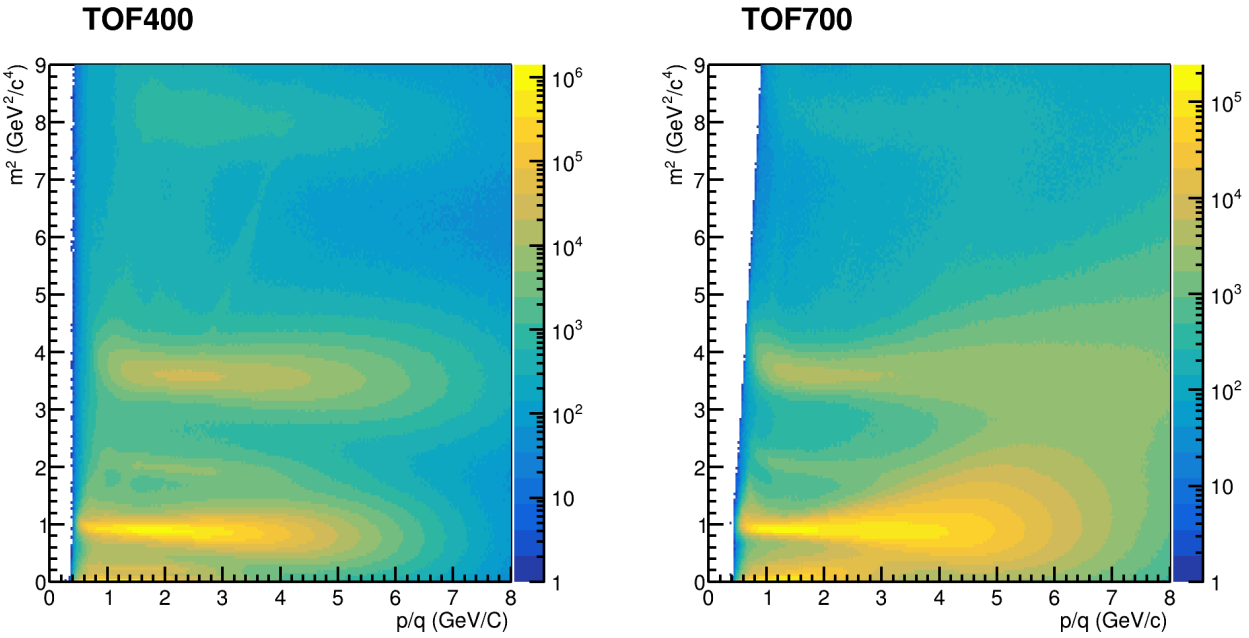

Figure 1: Population of the positively charged particles in the square mass m^2 vs. rigidity (p/q) plane for the TOF400 (left) and TOF700 (right).

Figure 6 shows the phase space coverage of identified deuterons as a function of rapidity y_{cm} and transverse momentum p_T for TOF-400, TOF-700 and for the combined system. Efficiency of the deuteron reconstruction was calculated using the realistic Monte-Carlo modelling of the BM@N experiment using GEANT4 transport code and DCM-QGSM-SMM model [11; 12]. Efficiency of the deuteron reconstruction with the TOF-detectors acceptance applied is shown in the Figure. 7.

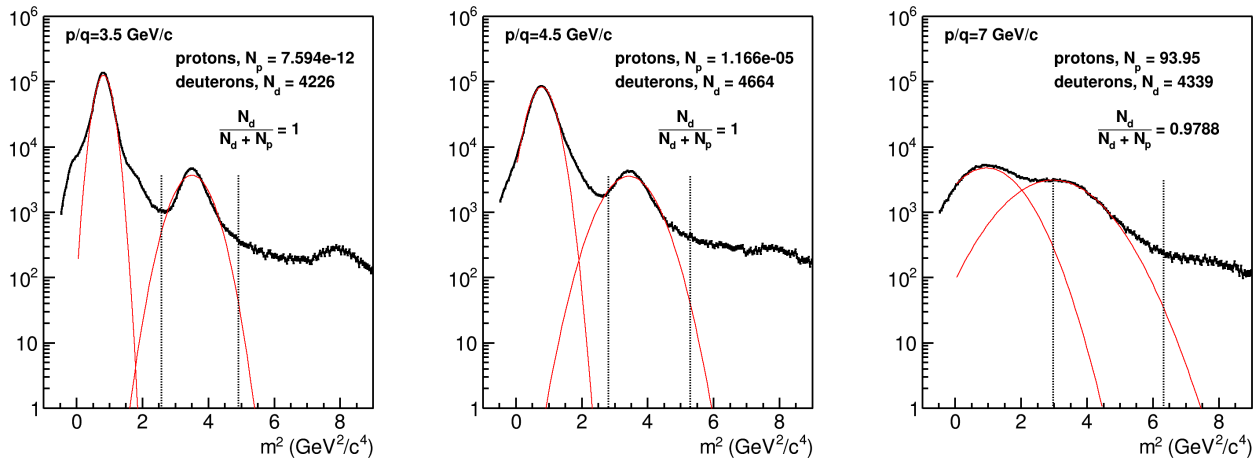

Figure 2: m^2 distribution of particles detected in the TOF700 for several rigidity (p/q) values. Red curves are approximations of the proton and deuteron peaks, and the vertical lines indicate the m^2 ranges for deuteron selection.

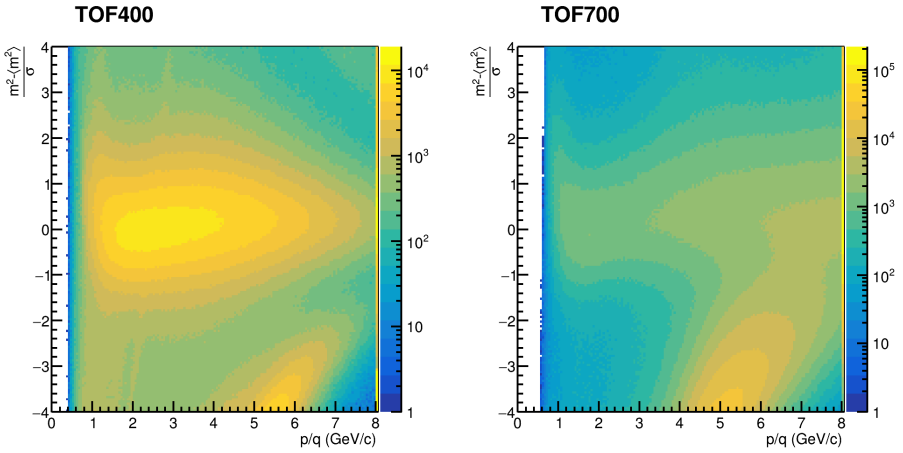

Figure 3: Population of charged particles in the n-sigma $(m_p^2) = (m^2\text{-}\langle m_d^2 \rangle)/\sigma_{m_d^2}$ vs. rigidity (p/q) plane for the TOF-400 (left) and TOF-700 (right) detectors.

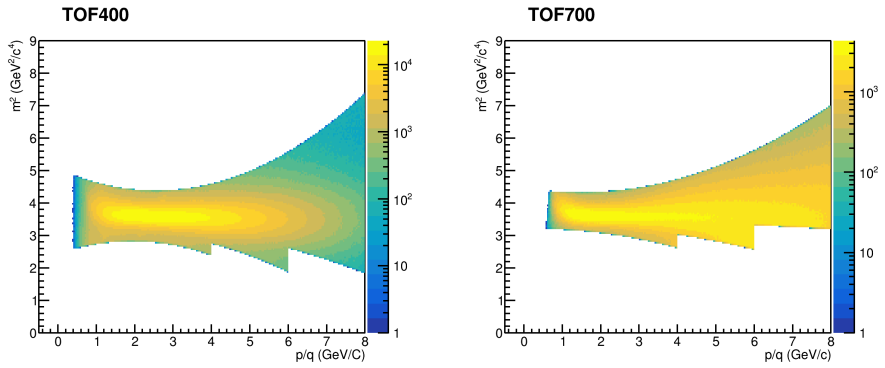

Figure 4: Population of selected deuterons in the m^2 vs. rigidity (p/q) plane for the TOF-400 (left) and TOF-700 (right) detectors. The deuteron selection criteria are shown in Table 2.

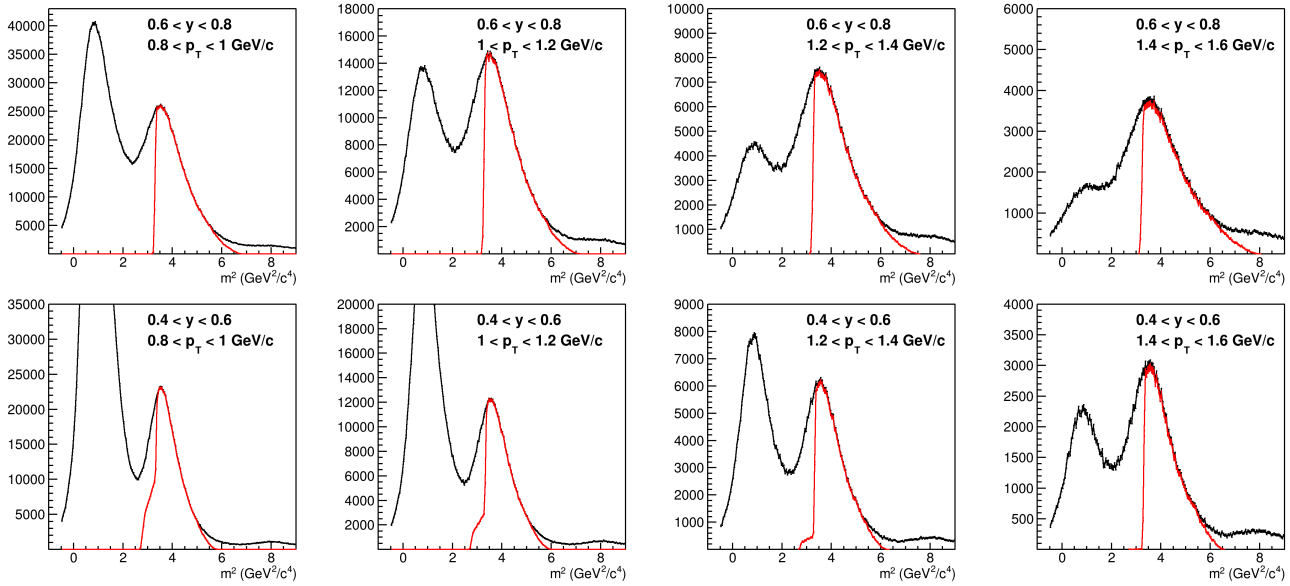

Figure 5: m^2 distribution of all particles (black line) detected in the TOF700 and of deuterons selected according to the n-sigma cuts (red line) for different y and p_T bins.

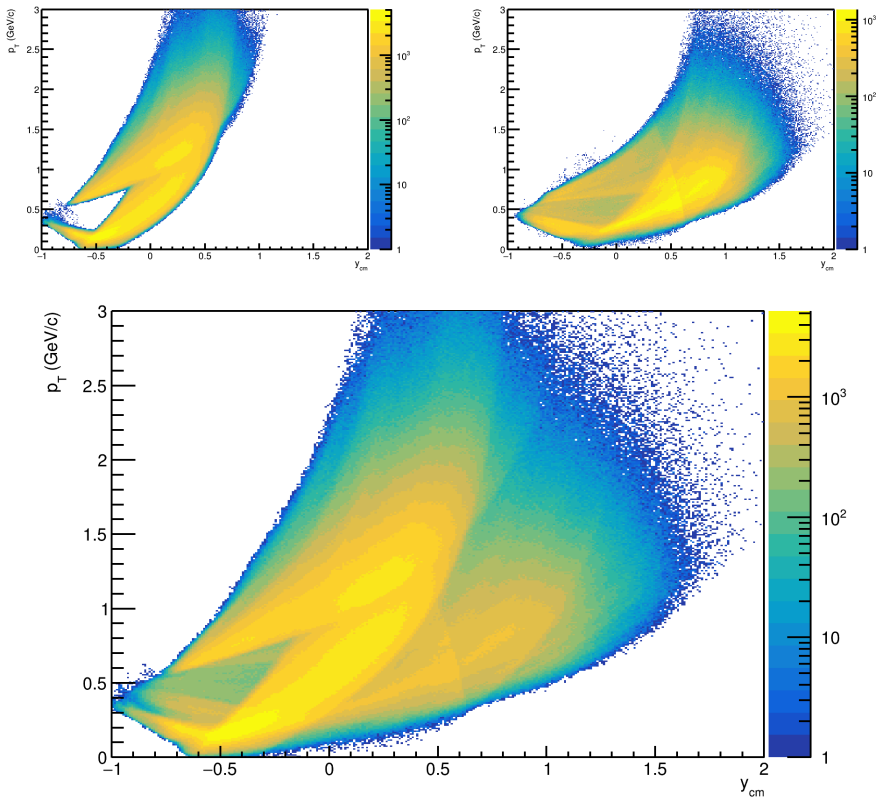

Figure 6: The phase space coverage of identified deuterons as a function of the centre-of-mass rapidity y_{cm} and transverse momentum p_T.

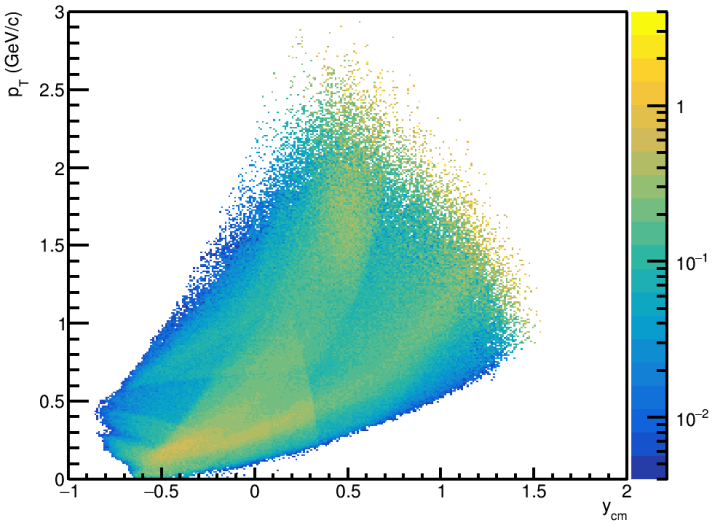

Figure 7: Efficiency of the deuteron reconstruction in the phase space of rapidity y_{cm} and transverse momentum p_T.

3 The analysis of v_1 of deuterons from BM@N run8 data

In this section, we discuss the details of analysis of directed flow v_1 of deuterons in Xe+Cs(I) collisions at 3.8 AGeV using the BM@N run8 data. The symmetry plane estimation and resolution correction factor calculation was performed identical to how it was done for the analysis of directed flow of protons, so for details on the u_n-Q_n-vector formalism, corrections on the azimuthal non-uniformity, BM@N performance for the flow measurements, please consult the [10].

1) To address the effects of the non-uniform acceptance we applied the corrections for both u_1 and Q_1 vectors :recentering, twist and rescaling. The QnTools framework [13] was used for corrections of u_1 and Q_1 vectors and flow analysis. For u_1-vector corrections were employed multi-differentially on transverse p_T, rapidity y and centrality. For the Q_1-vectors corrections were applied only differentially on centrality.

2) The detailed performance study [10] shows that due to magnetic field acting along the y-axis and deflecting charged particles along the x axis, we can measure the directed flow v_1 of protons using only the y components of flow vectors:

$$v_1 = 2\frac{\langle y_1 Y_1^a \rangle}{R_1^y\{a\}}, \tag{4}$$

where the resolution correction factor is calculated using the method of three sub-events:

$$R_1^y\{a(b,c)\} = \sqrt{\frac{\langle Y_1^a Y_1^b \rangle \langle Y_1^a Y_1^c \rangle}{\langle Y_1^b Y_1^c \rangle}}, \tag{5}$$

or by the four sub-event method:

$$R_1^y\{a(d)(b,c)\} = \langle Y_1^a Y_1^d \rangle \sqrt{\frac{\langle Y_1^d Y_1^b \rangle \langle Y_1^d Y_1^c \rangle}{\langle Y_1^b Y_1^c \rangle}}, \tag{6}$$

3) The Y_1 component of the Q_1 vector for symmetry planes in the FHCal have been obtained using the formula:

$$Y_1 = \frac{\sum_{k=1}^{M} E_k \sin(\phi_k)}{\sum_{k=1}^{M} E_k} \tag{7}$$

, where E_k and ϕ_k is the energy deposition and azimuthal angle of the k-th module and M is the number of modules used.

Modules of the FHCal were divided into three groups (sub-events): F1, F2, F3 as it is shown in the Figure. 8. According to the simulations, due to charge splitting in the dipole analyzing magnet SP-41, F1 sub-event primarily registers the spectator protons, F2 — spectator fragments and F3 — neutrons.

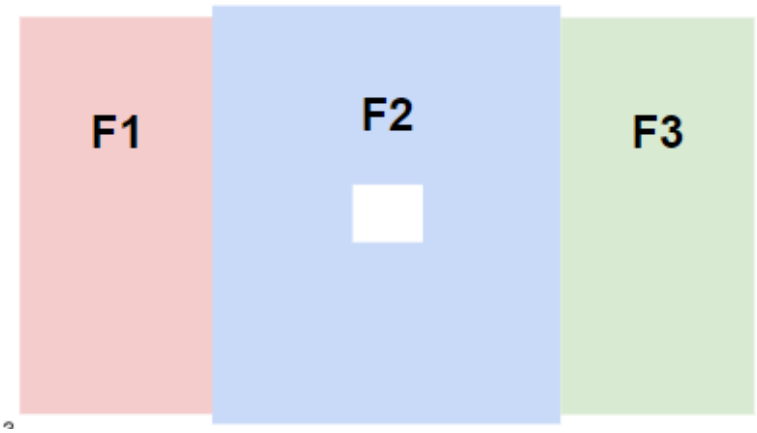

Figure 8: Layout of the FHCal modules division into three groups (sub-events): F1, F2, F3.

Two additional sub-events were introduced from the tracks of the charged particles in the inner tracking system of BM@N. All negatively charged particles with pseudorapidity $1.5 < \eta < 3$ and transverse momentum $p_T > 0.2$ GeV/c comprise the T- sub-event. The T+ sub-event consists of positively charged particles in following kinematic region: $2 < \eta < 3$ and $p_T > 0.2$ GeV/c.

Resolution correction factor was calculated for 3 spectator symmetry planes F1, F2, and F3 using the three sub-event method (for F2 four sub-event technique was employed as well) using the Equation 5 (and for four sub-events Equation 6). Figure 9 shows the centrality dependence of the resolution correction factors R_1 for sub-event symmetry planes F1, F2 and F3 from left to right. For each symmetry plane R_1

was estimated using 3 combinations of sub-events (as indicated in the figure). One can observe that all three estimations for each symmetry plane are in reasonable agreement. This fact may suggest that the contribution of non-flow correlations in the final values of R_1 is very small. The R_1 for all three symmetry planes calculated using $T-$ sub-event is off in the last centrality bin (30-40%) due to the fact that directed flow of negatively charged pions crosses zero at this centrality. We employ this estimation purely for the verification purpose and this outlier does not affect the estimated values for v_1. For correction on the symmetry plane resolution we use $F1(F2, F3)$, $F2(F1, F3)$ and $F3(F1, F2)$ combinations.

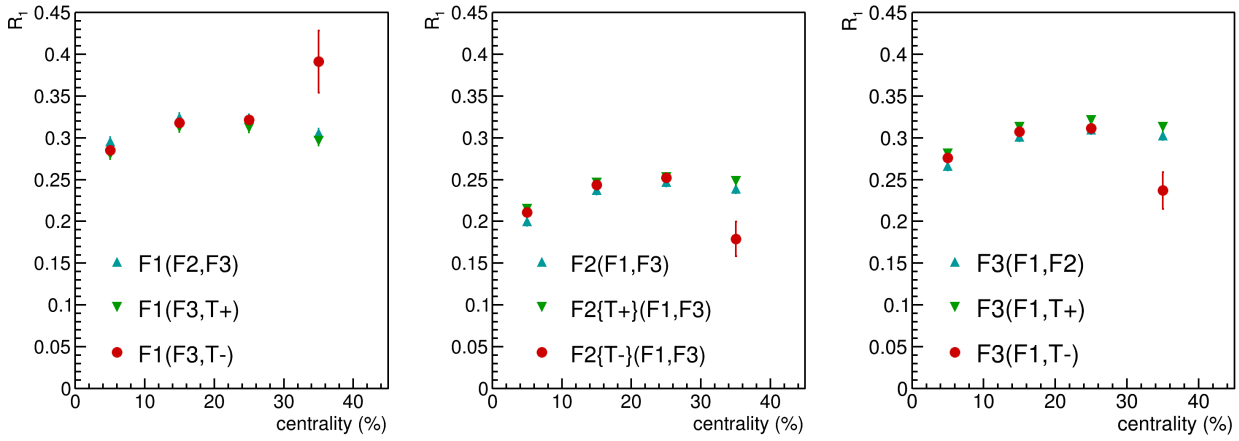

Figure 9: Resolution correction factor R_1 calculated using different combinations as a function of centrality for sub-event symmetry planes F1, F2 and F3 from left to right.

4) Figure 10 shows the rapidity dependence y_{cm} of directed flow v_1 of deuterons in in 10-30% central Xe+Cs(I) collisions at 3.8 A GeV. The measurements have been performed with respect to the F1, F2, F3 and combined(F2+F3) symmetry planes. The resulting v_1 values of deuterons are in a good agreement for the measurements with respect to F2, F3 and combined(F2+F3) symmetry planes. The small difference in resulting v_1 values for the measurements with respect to the F1 plane, can be explained by the small contribution of non-flow effects. In order to get the final results, the measurements of directed flow v_1 have been performed with respect to the combined (F2+F3) symmetry plane, see Figure 17.

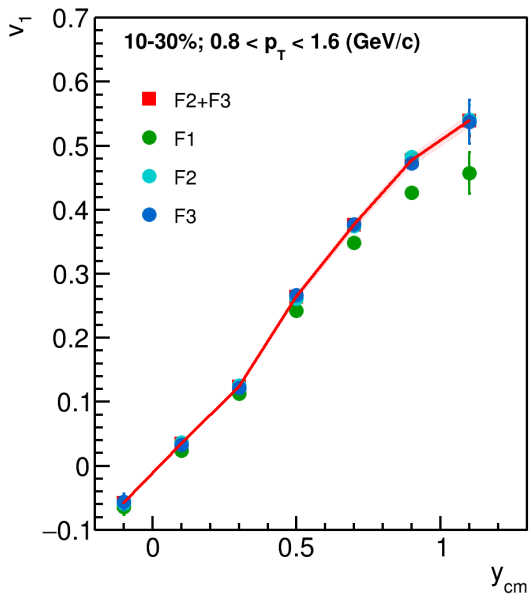

Figure 10: Directed flow v_1 of deuterons as a function of rapidity y_{cm} measured with respect to different spectator symmetry planes: F1, F2, F3 and combined (F2+F3), see text for the details.

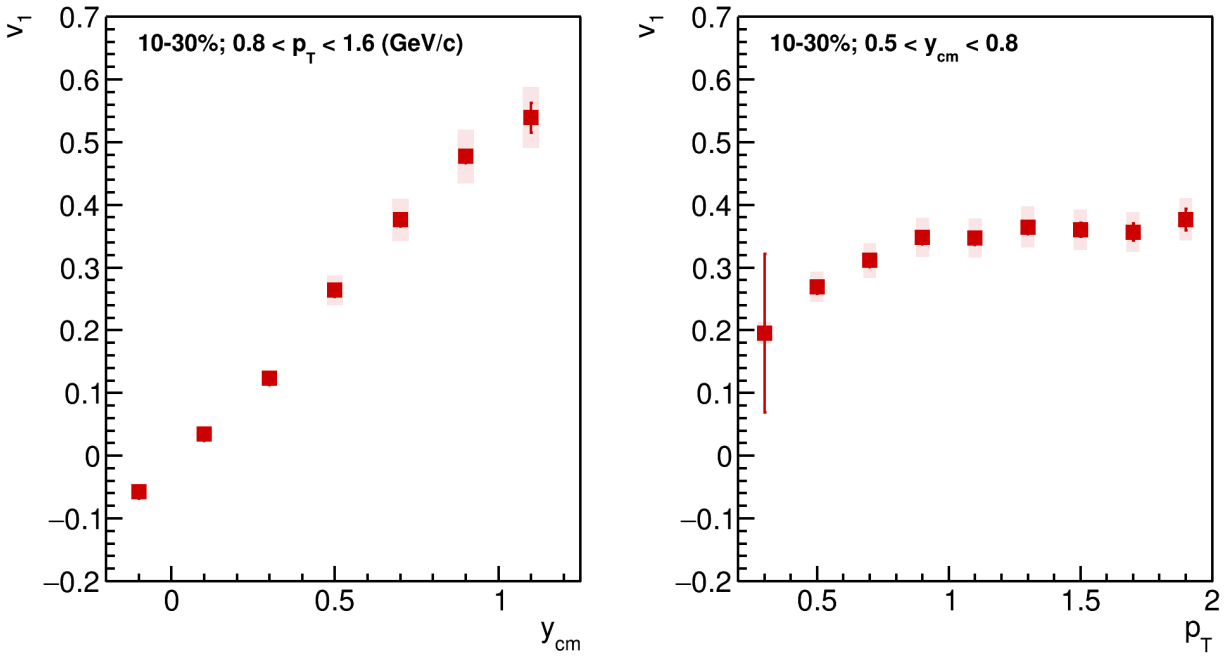

Figure 11: Directed flow v_1 of deuterons in 10-30% central Xe+Cs(I) collisions at 3.8 A GeV as a function of rapidity y_{cm} (left panel) and transverse momentum p_T (right panel).

4 Systematic uncertainties of v_1 measurements

In order to estimate systematic uncertainties of v_1 measurements , the following sources were considered:

- Uncertainty in deuteron momentum reconstruction. We varied the number of stations N_{hits} in inner tracking system used for track reconstruction as well as the values of track χ^2/NDF quality, see results in Figure 12. The overall systematic uncertainty is found to be below 5%.

- Contribution from the secondary particles. We studied the difference in v_1 results for tracks with different Distance of the Closes Approach (DCA) to the primary vertex, see the left panel of Figure 13 for results. It is found that deuteron v_1 values obtained with different DCA cut are in agreement within 1-2%.

- Contamination from the different particle species. We used stricter criteria for deuteron selection in TOF700 , which are: $-2\sigma < (m^2 - \langle m^2 \rangle) < 2.5\sigma$ for $0 < p/q < 4$ GeV/c; $-0.5\sigma < (m^2 - \langle m^2 \rangle) < 2.5\sigma$ for $4 < p/q < 6$ GeV/c; $0.5\sigma < (m^2 - \langle m^2 \rangle) < 2.5\sigma$ for $6 < p/q < 8$ GeV/c. See the right panel of Figure 13 for results. Observed is the systematic uncertainty below 5%

- Contribution due to off-target collisions. We divided the events based on the azimuthal angle of the vertex position and compared the v_1 of deuterons in each group of events, see results in Figure 14. Systematic variation stays below 3%.

- Acceptance and efficiency. We perform the v_1 flow measurements for deuterons identified with TOF-400 and TOF-700 separately. We perform the measurements with and without the applying the efficiency correction for deuterons based on MC simulations for run8, see Figure 15 for results. The results are in a good agreement and we can conclude that the mean value of transverse momentum p_T is not shifted in this rapidity range.

- Run-by-run systematics was estimated dividing the events into several run periods and comparing the results in each group, see the left panel of Figure 16

for results. The systematic uncertainty is less than 5% and found to be less than statistical.

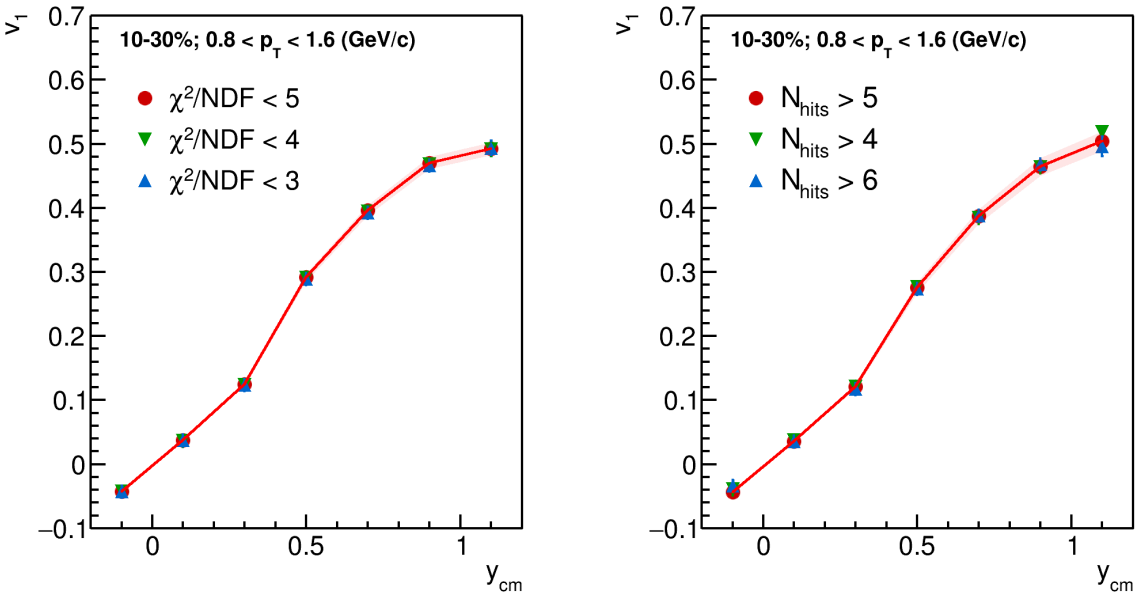

Figure 12: Directed flow v_1 of deuterons as a function of rapidity y_{cm} measured for different values of the track χ^2/NDF quality (left) and the number of stations used for track reconstruction N_{hits} (right).

Systematic uncertainties were calculated by the square root of quadratic sum of uncertainties from each source.

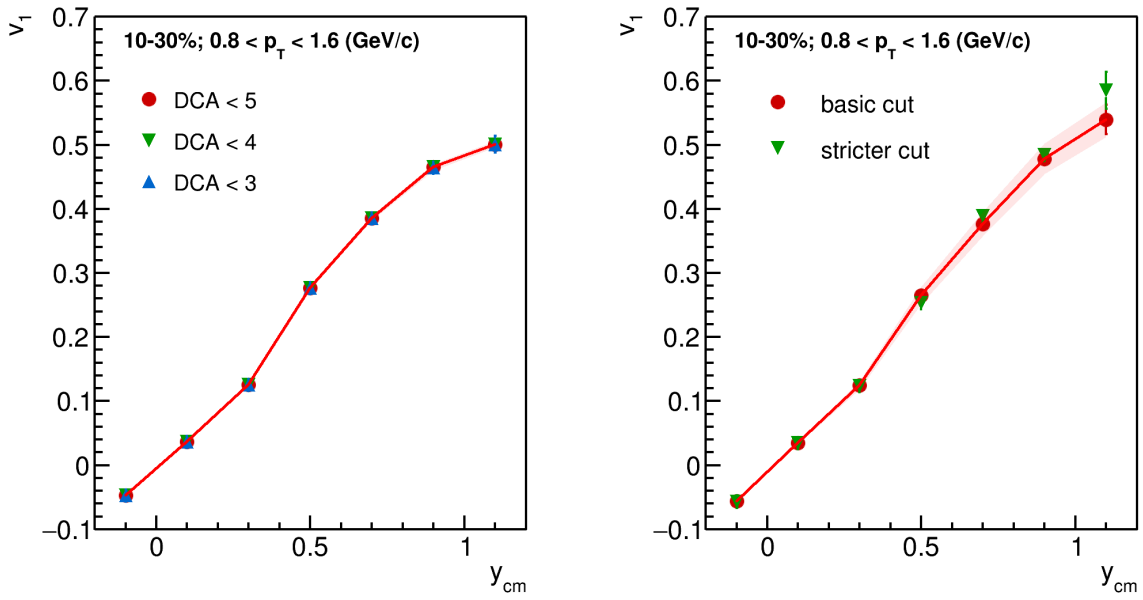

Figure 13: Directed flow v_1 of deuterons as a function of rapidity y_{cm} measured for different values of the DCA cut and different n-σ PID cuts for the deuteron identification: $(m^2\text{-}\langle m_p^2 \rangle) < 1, 2, 3\ \sigma_{m_p^2}$ cut (right).

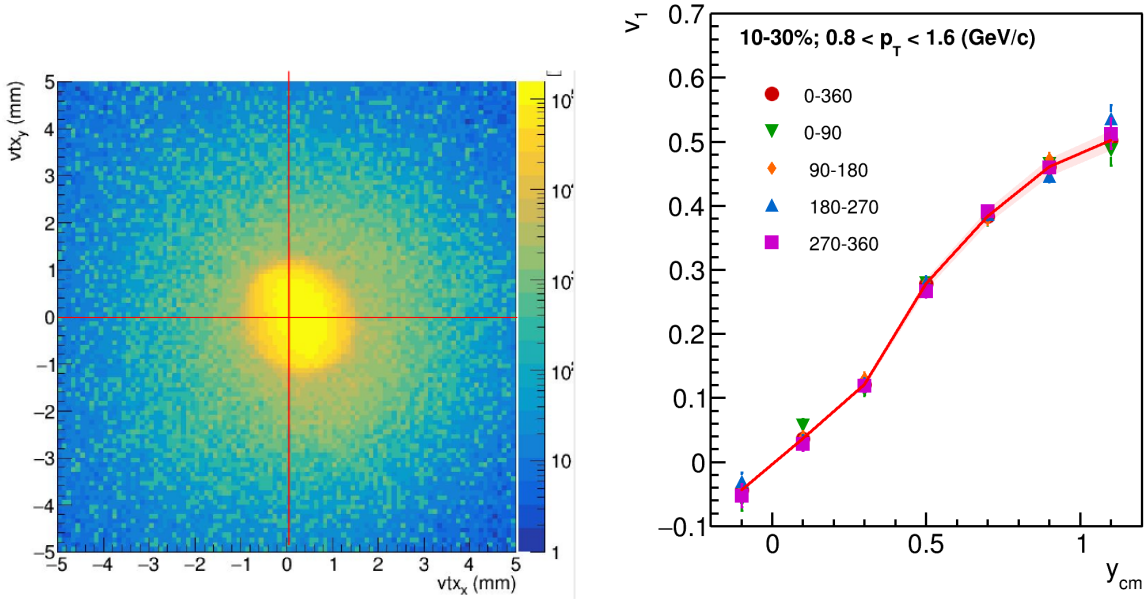

Figure 14: Left: the distribution of the primary vertex in X-Y plane. Right: Directed flow v_1 of deuterons as a function of rapidity y_{cm} calculated with varying the reconstructed primary vertex position of the collision.

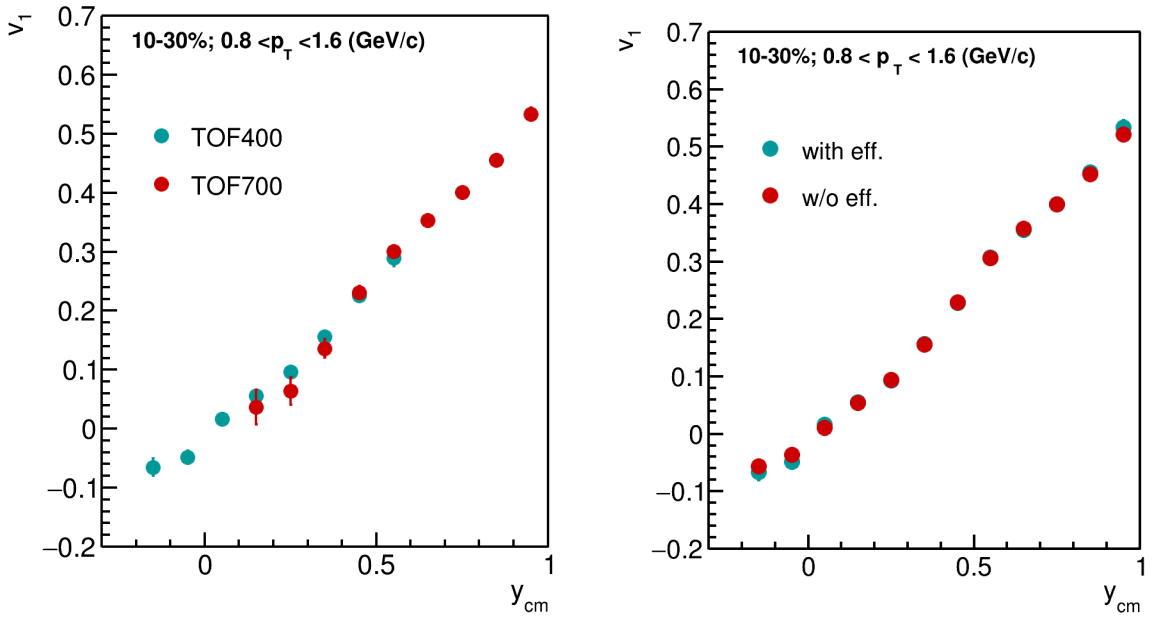

Figure 15: Directed flow v_1 of deuterons as a function of rapidity y_{cm} measured for deuterons identified using different TOF-systems (left) and deuterons weighted and not weighted with efficiency based on MC simulations for run8 (right).

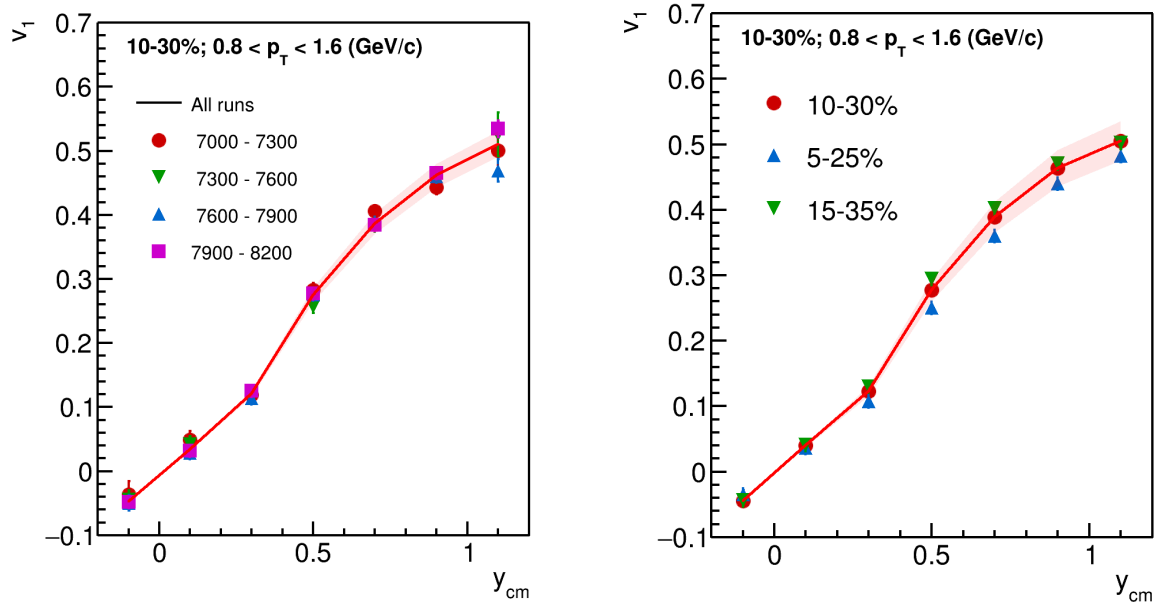

Figure 16: Directed flow v_1 of deuterons as a function of rapidity y_{cm} measured in the different run periods (left) and for different bins in collision centrality (right).

5 Results of the directed flow measurements

Directed flow v_1 of deuterons was measured in 10-30% central Xe+Cs(I) collisions at 3.8 AGeV as a function of rapidity y_{cm} and transverse momentum p_T, see Figure. 17. Rapidity-dependence and transverse-momentum-dependence of v_1 of deuterons from the experimental data has been compared with proton v_1 obtained for the same data [10]. The directed flow of deuterons is greater that that of protons as was expected.

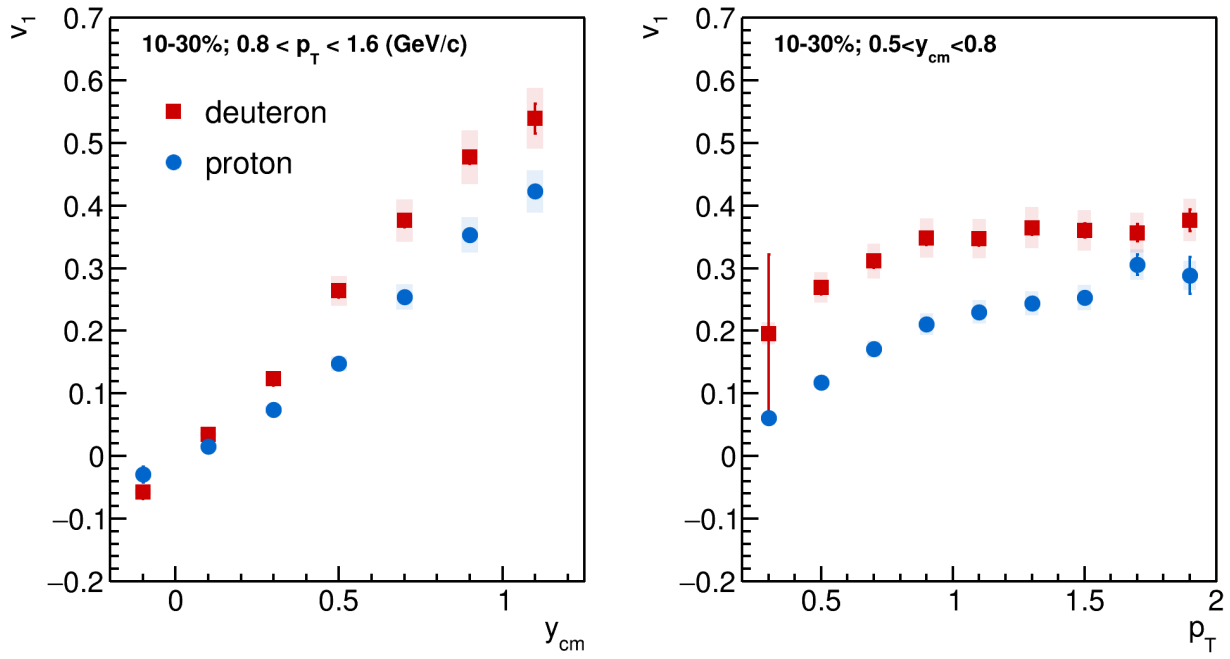

Figure 17: Directed flow v_1 of deuterons in 10-30% central Xe+Cs(I) collisions at 3.8 A GeV as a function of rapidity y_{cm} (left panel) and transverse momentum p_T (right panel).

The coalescence scaling was studied similar to how it was done by the STAR experiment [8]. The directed flow of light nuclei is divided over a respective mass number A together with the transverse momentum. The underlying assumption is that nucleons with similar momenta can strongly bind producing the corresponding light nuclei such as deuterons, tritons, helium-3 and etc. Directed flow of protons and deuterons before (upper plots) and after (lower plots) applying the scaling in different rapidity bins is shown in fig. 18. We observe that v_1 of light nuclei follow the scaling in selected rapidity ranges.

The slope of the directed flow v_1 at midrapidity $dv_1/dy_{cm}|_{y_{cm}=0}$ is extracted by fitting the $v_1(y_{cm})$ with polynomial function $v_1 = a + by_{cm} + cy_{cm}^3$ as it was done in other experiments [14–17]. The slope of v_1 of deuterons at midrapidity $dv_1/dy_{cm}|_{y_{cm}=0}$ as a function of collision energy is presented in the fig. 19. The results for the BM@N experiment are compared with existing data from other experiments [15–17]. Directed flow slope at midrapidity $dv_1/dy_{cm}|_{y_{cm}=0}$ are found to be in a reasonable agreement with the existing measurements.

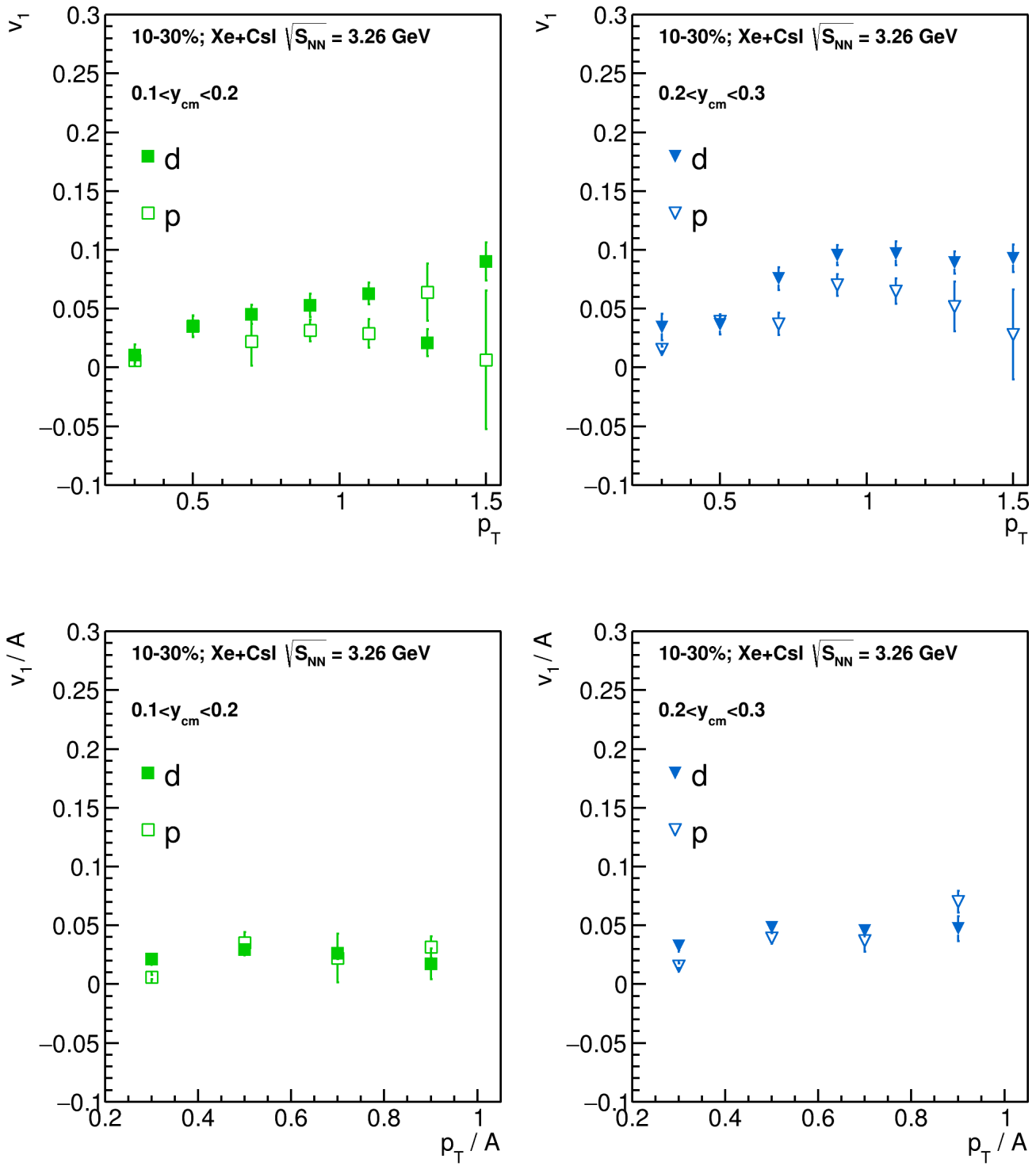

Figure 18: Upper plots: directed flow v_1 of protons and deuterons in 10-30% central Xe+Cs(I) collisions at 3.8 A GeV as a function of transverse momentum p_T. Lower plots: directed flow scaled on the corresponding mass number v_1/A for protons and deuterons in 10-30% central Xe+Cs(I) collisions at 3.8 A GeV as a function of scaled transverse momentum p_T/A.

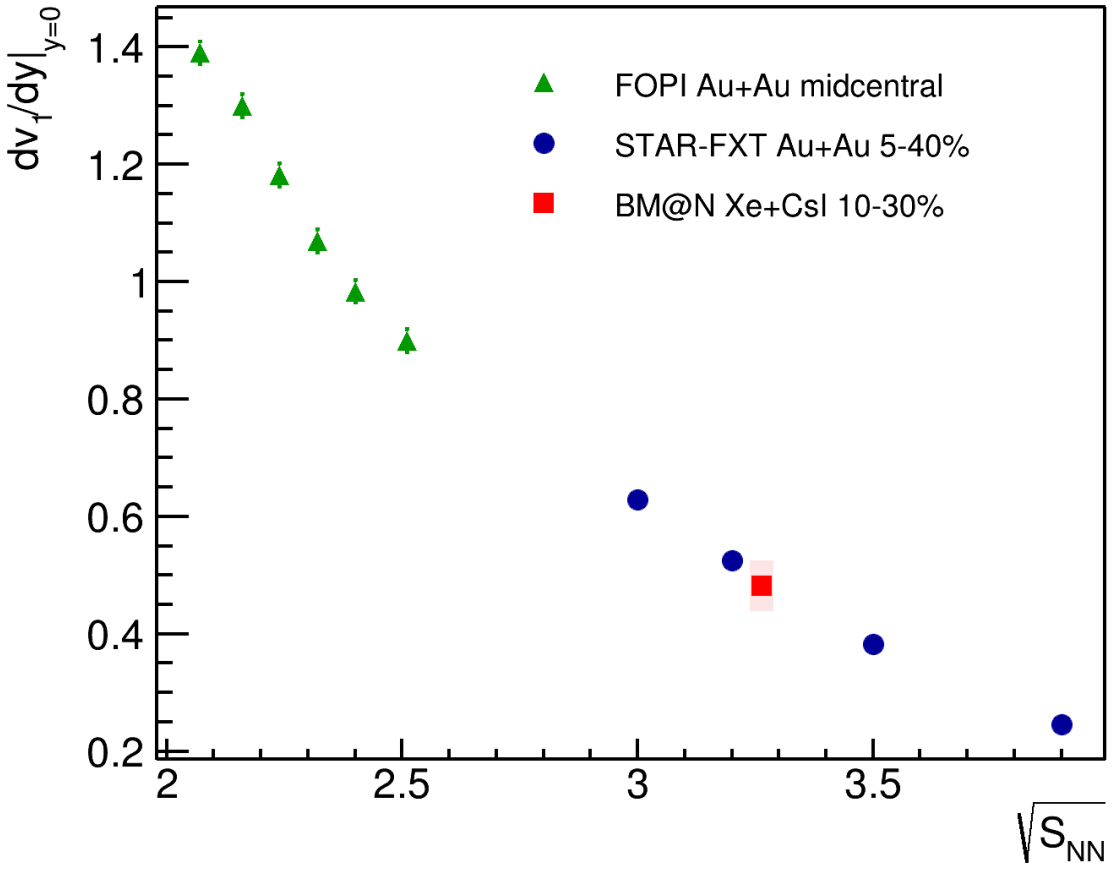

Figure 19: The slope of v_1 of deuterons at midrapidity $dv_1/dy_{cm}|_{y_{cm}=0}$ as a function of collision energy. The obtained BM@N results were compared with existing data from other experiments [15–17].

References

1. *Poskanzer A. M.*, *Voloshin S. A.* Methods for analyzing anisotropic flow in relativistic nuclear collisions // Phys. Rev. C. — 1998. — Vol. 58. — P. 1671–1678.

2. *Voloshin S.*, *Zhang Y.* Flow study in relativistic nuclear collisions by Fourier expansion of azimuthal particle distributions // Zeitschrift for Physik C Particles and Fields. — 1996. — May. — Vol. 70, no. 4. — P. 665–671.

3. *Shen C.*, *Heinz U.* The road to precision: Extraction of the specific shear viscosity of the quark-gluon plasma // Nucl. Phys. News. — 2015. — Vol. 25, no. 2. — P. 6–11. — arXiv: `1507.01558 [nucl-th]`.

4. *Herrmann N.*, *Wessels J. P.*, *Wienold T.* Collective flow in heavy ion collisions // Ann. Rev. Nucl. Part. Sci. — 1999. — Vol. 49. — P. 581–632.

5. *Zhang C.* [et al.]. Beam energy dependence of the squeeze-out effect on the directed and elliptic flow in Au + Au collisions in the high baryon density region // Phys. Rev. C. — 2018. — Vol. 97, no. 6. — P. 064913.

6. *Adamczewski-Musch J.* [et al.]. Probing dense baryon-rich matter with virtual photons // Nature Phys. — 2019. — Vol. 15, no. 10. — P. 1040–1045.

7. *Danielewicz P.*, *Lacey R.*, *Lynch W. G.* Determination of the equation of state of dense matter // Science. — 2002. — Vol. 298. — P. 1592–1596.

8. *Abdallah M.* [et al.]. Light nuclei collectivity from sNN=3 GeV Au+Au collisions at RHIC // Physics Letters B. — 2022. — Vol. 827. — P. 136941. — ISSN 0370-2693.

9. *Afanasiev S.* [et al.]. The BM@N spectrometer at the NICA accelerator complex. — 2023. — Dec. — arXiv: `2312.17573 [hep-ex]`.

10. *Mamaev M.* [et al.]. Directed flow v_1 of protons in the Xe+Cs(I) collisions at 3.8 AGeV (BM@N run8). —. — eprint: `https://indico.jinr.ru/event/4750/attachments/19780/34163/ANoteFlowRun8.pdf`.

11. *Baznat M.* [et al.]. Monte-Carlo Generator of Heavy Ion Collisions DCM-SMM // Phys. Part. Nucl. Lett. — 2020. — Vol. 17, no. 3. — P. 303–324. — arXiv: 1912.09277 [nucl-th].

12. *Botvina A. S.* [et al.]. Multifragmentation of spectators in relativistic heavy ion reactions // Nucl. Phys. A. — 1995. — Vol. 584. — P. 737–756.

13. *Selyuzhenkov I.*, *Kreis L.* QnTools -A framework for multi-differential acceptance correction and anisotropic flow analysis // https://github.com/HeavyIonAnalysis/Q 2024.

14. *Adamczewski-Musch J.* [et al.]. Proton, deuteron and triton flow measurements in Au+Au collisions at $\sqrt{s_{\rm NN}} = 2.4$ GeV // Eur. Phys. J. A. — 2023. — Vol. 59, no. 4. — P. 80.

15. *Sharma S. R.* First-Order Event Plane Correlated Directed and Triangular Flow from Fixed-Target Energies at RHIC-STAR // Universe. — 2024. — Vol. 10, no. 3. — P. 118.

16. *Abdallah M. S.* [et al.]. Disappearance of partonic collectivity in $\sqrt{s_{\rm NN}} = 3$ GeV Au+Au collisions at RHIC // Phys. Lett. B. — 2022. — Vol. 827. — P. 137003.

17. *Reisdorf W.* [et al.]. Systematics of azimuthal asymmetries in heavy ion collisions in the 1 A GeV regime // Nucl. Phys. A. — 2012. — Vol. 876. — P. 1–60.